A First-Order Model for Depolarization of Propagating Signals by Narrowband Ricean Fading Channels

Kyle N. Sivertsen, *Student Member, IEEE,* Anthony E.-L. Liou, *Student Member, IEEE,* Arghavan Emami-Forooshani, *Student Member, IEEE,* and David G. Michelson, *Senior Member, IEEE*

***Abstract*—We show by simulation that when the fading signals observed on orthogonally polarized diversity branches follow Ricean statistics, the distribution of polarization states on the Poincaré sphere is well-approximated by a Fisher distribution. Further, we show that the Fisher concentration parameter is: (1) completely determined by the corresponding Ricean K-factors and the cross-correlation coefficient between the diversity branches, both of which can be estimated from simple measurements of received power vs. time, and (2) a good indicator of the level of cross-polar discrimination (XPD) on the channel. The insights gained are potentially useful to those engaged in the development and validation of schemes that use either polarization re-use or polarized MIMO.**

***Index Terms*—Channel model, cross-polar discrimination, fading channel, polarimetry, polarization diversity.**

I. INTRODUCTION

POLARIZATION diversity on narrowband fixed wireless links has traditionally been characterized in terms of the fading statistics and the cross-correlation between the Rician distributed signals on each branch, e.g., [1]. A complementary approach, which provides additional physical insight and which is independent of the polarization states of the diversity receiving antennas, is to characterize the manner in which the polarization states observed at the receiver disperse across the Poincaré sphere. In the absence of fading, the polarization state of the signal that is observed at the receiver will describe a single point. As the depth of fading increases and as the correlation between the signals observed on the diversity receiving branches decreases, the polarization states observed by the receiver will begin to disperse. In the limit as fading on the branches becomes uncorrelated and Rayleigh, the polarization states will be uniformly distributed across the sphere.

The notion that it may be useful to consider the manner in which the polarization states associated with wireless signals disperse across the Poincaré sphere has previously been considered, e.g., [2] and [3]. To the best of our knowledge, however, we are the first to consider the statistics of polarization state dispersion by Ricean fading channels. The polarization state distribution that one expects to see at the receiving antenna is of particular interest to those engaged in the simulation and test of polarization diversity schemes or polarization adaptive antennas. Knowledge of the polarization state distribution also allows one to estimate the level of cross-polar discrimination (XPD) on the channel. Such information is of particular interest to those engaged in the development and evaluation of polarization re-use or polarized MIMO schemes, e.g., [4],[5].

In this work, we show: (1) that the manner in which polarization states disperse across the Poincaré sphere over time, i.e., the first-order statistics of dispersion, is well-described by a spherical normal or Fisher distribution and (2) how the parameters of this distribution are related to the narrowband channel parameters that describe the diversity channel. We also show how knowledge of the polarization state distribution might be used to predict the level of XPD on the channel.

The remainder of this paper is organized as follows: In Section II, we describe the concept in greater detail and explain our methodology. In Section III, we show how dispersion of polarization states over time is related to the conventional narrowband channel parameters. In Section IV, we show that the dispersion of polarization states is closely correlated with XPD. In Section V, we summarize our contributions and their implications.

II. CONCEPT AND METHODOLOGY

In [1], it was shown that the first-order statistics of the Ricean fading signals $g_1(t)$ and $g_2(t)$ observed on diversity receiving branches are completely described by: (1) the average path gains G and Ricean K-factors K observed on each branch and (2) the cross-correlation coefficient ρ between the time varying components of the signals on each receiving branch. In such cases,

$$g_1(t) = \sqrt{\frac{G_1}{K_1+1}}\left[\sqrt{K_1} + x_1(t)\right] \tag{1}$$

and

$$g_2(t) = \sqrt{\frac{G_2}{K_2+1}}\left[\sqrt{K_2}e^{j\Delta\Psi} + x_2(t)\right], \tag{2}$$

where $x_1(t)$ and $x_2(t)$ are zero-mean complex Gaussian processes with unit standard deviations and $\Delta\Psi$ is the phase offset between the fixed components of $g_1(t)$ and $g_2(t)$ that may result from the relationship between the transmit and receive polarizations.

We denote the correlation between the complex Gaussian variates x_1 and x_2 by

$$\rho = \overline{x_1 x_2^*} = Re^{j\theta}. \tag{3}$$

Manuscript received March 11, 2008; revised July 27, 2008 and January 18, 2009; accepted January 22, 2009. The associate editor coordinating the review of this letter and approving it for publication was R. Murch.

The authors are with the Radio Science Lab, Department of Electrical and Computer Engineering, University of British Columbia, Vancouver, BC, Canada, V6T 1Z4 (e-mail: {ksiverts, eliou, arghavan, davem}@ece.ubc.ca).

This work was supported in part by grants from Bell Canada and Western Economic Diversification Canada.

Digital Object Identifier 10.1109/TWC.2009.081001

If the phase between the fixed components is assumed to be zero, the power correlation coefficient ρ_{pwr} between the envelopes of g_1 and g_2 is related to $Re^{j\theta}$ by

$$\rho_{pwr} = \frac{R^2 + 2\mu_c\sqrt{K_1K_2}}{\sqrt{(1+2K_1)(1+2K_2)}}, \tag{4}$$

where μ_c the real part of the complex correlation coefficient and is given by

$$\mu_c = R\cos\theta, \tag{5}$$

as described in [6] and [7]. In the remainder of this paper, we use ρ_{pwr} to indicate the degree of cross-correlation between diversity branches.

When the angle of arrival distribution is sufficiently narrow that the antenna pattern appears to be constant over the range, e.g., as one might observe at a base station in a macrocell environment or at the satellite end of an earth-space link, the polarization state of the signal observed at the receiver at a given instant can be determined from knowledge of the amplitude and phase of the signals received on orthogonally polarized branches at that instant. The arctangent of the ratio of the signal amplitudes gives the polarization angle γ while the difference between the signal phases gives the polarimetric phase δ. Trigonometric expressions that relate the polarization angle and polarimetric phase to the ellipticity angle ϵ and tilt angle τ that define the polarization ellipse can be derived using spherical trigonometry, as described in [8].

The amplitude distribution of a Ricean signal with a given K-factor and mean received power Ω is given by the well-known expression

$$\begin{aligned} p(r) =& \frac{2r\,(K+1)}{\Omega} exp\left(-K - \frac{r^2\,(K+1)}{\Omega}\right) \\ &\cdot I_0\left(2r\sqrt{\frac{K\,(K+1)}{\Omega}}\right), \end{aligned} \tag{6}$$

where $I_0(z)$ is the modified Bessel function of the first kind of order zero. The phase distribution of a Ricean signal is given by

$$\begin{aligned} p(\vartheta) =& \frac{1}{2\pi}e^{-K}\left[1+\sqrt{K\pi}\cos\vartheta e^{K\cos^2\vartheta}\right. \\ &\left.\cdot\left(1+erf\left(\sqrt{K}\cos\vartheta\right)\right)\right] \end{aligned} \tag{7}$$

where

$$erf\,(G) = \frac{2}{\sqrt{\pi}}\int_0^G e^{-y^2}dy. \tag{8}$$

Although one could derive closed form expressions for the polarization angle and polarimetric phase distributions using (6) and (7), the effort required would be considerable. We therefore opted to use numerical simulations to determine the manner in which the polarization states of the received signal disperse across the Poincaré sphere over time.

Polarization diversity receiving antennas are usually chosen to be both symmetrically and orthogonally polarized. For example, when the transmitted signal is vertically polarized, we might use forward and back slanted diagonally polarized receiving antennas. The inherent symmetry suggests that the fading statistics on the two channels might reasonably be assumed to be identical, i.e., identical path gains G and Ricean K-factors K. We refer to this as an ideal Ricean diversity channel. By assuming such a channel, we can reduce the number of independent first-order channel model parameters to just three: G, K and ρ_{pwr}.

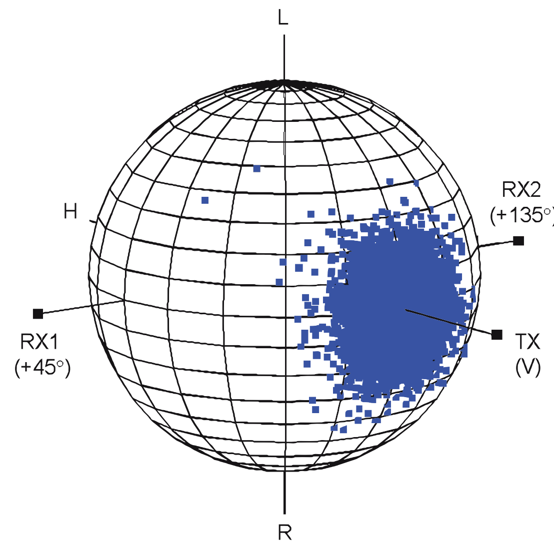

Fig. 1. Dispersion of polarization states on the Poincaré sphere when fading signals observed on the forward and back-slant polarized receiving antennas RX1 and RX2 are characterized by $K = 10$ dB and $\rho_{pwr} = 0.8$. The transmitted signal was vertically polarized but has been depolarizd by the environment.

Because the average path gains G on the two branches are identical, they cancel out when we calculate the polarization ratio and therefore do not affect the polarization state. For each instance of K and ρ_{pwr} that we considered, we generated almost 10,000 values of $g_1(t)$ and $g_2(t)$ using a cross-correlated Ricean channel simulator [9]. From the ratio $g_1(t)/g_2(t)$ at a given instant, we determined the polarization angle γ and the polarimetric phase δ, or, alternatively, the ellipticity and tilt angles, ϵ and τ, that define the polarization state of the received signal. Finally, we plotted the polarization states on a Poincaré sphere, as suggested by Figure 1, where the longitude coordinate $\varphi' = 2\tau$ and the co-latitude coordinate $\theta' = 90 - 2\epsilon$ in degrees. The polarization states corresponding to horizontal and vertical, right and left circular, and $\tau = +45$ (forward slant) and +135 (back slant) with $\epsilon = 0$ are indicated.

III. Results

The manner in which polarization states are distributed across the Poincaré sphere for various K and ρ_{pwr} is presented in Figure 2. In order to facilitate assessment of the rotational symmetry of the distributions, we have rotated the spherical coordinate frame used in Figure 1 so that the polarization state corresponding to the mean direction of the distribution is coincident with one of the poles of the rotated coordinate frame. For ease of visualization as the distribution broadens, we displayed the rotated Poincaré sphere using Lambert's equal area azimuthal projection. Because this projection maps equal areas on the sphere onto equal areas on the plane, it preserves the density of polarization states. The centre of each plot in Figure 2 corresponds to vertical polarization while the outer circle corresponds to horizontal polarization.

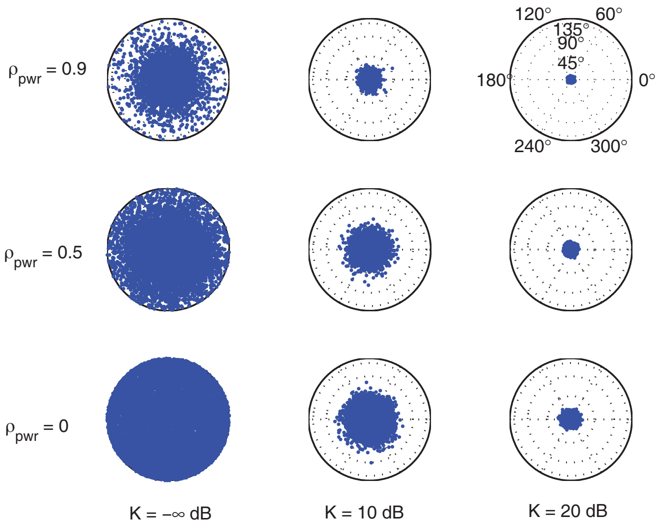

Fig. 2. Dispersion of polarization states on a Lambert equal area azimuthal projection of the Poincaré sphere when the fading signals observed on forward and back slant polarized receiving antennas are characterized by the indicated values of K [dB] and ρ_{pwr}.

The polarization state distributions in Figure 2 may be considered as the result of a correlated random walk. When K is very large, the polarization state distribution is confined to a sufficiently small portion of the sphere in the vicinity of the transmitter polarization state that it may effectively be considered a plane. In such cases, the central limit theorem predicts that the distribution will tend to conform to a two-dimensional isotropic Gaussian distribution. When K approaches $-\infty$, the polarization state distribution is unconstrained and covers the entire sphere. In such cases, the central limit theorem predicts that the random walk will conform to a spherical uniform distribution.

No general theory of correlated random walks on a sphere yet exists to guide us when considering intermediate values of K. However, the behavior of the polarization state distribution for very large and small values of K is very similar to that exhibited by the Fisher or spherical normal distribution given by

$$f(\theta, \phi) = \frac{\kappa \sin\theta}{2\pi (e^{\kappa} - e^{-\kappa})} e^{\kappa(\sin\theta \sin\alpha \cos(\phi-\beta) + \cos\theta \cos\alpha)} \quad (9)$$

for very large and small values of κ, respectively. Here, θ and ϕ are the co-latitude and longitude (elevation and azimuth angle) in the local spherical coordinate frame, κ is the concentration parameter, and α and β are the co-latitude and longitude, respectively, of the mean direction of the polarization state distribution [10]. If the polarization state distributions for arbitrary values of K and ρ_{pwr} are, in fact, well approximated by Fisher distributions with appropriate values of κ, effective methods for compactly representing and simulating such distributions become available. In particular, methods for simulating pseudo random samples of the Fisher distribution which, by extension, may be used to simulate polarization state distributions, are presented in [11]-[13].

If the mean direction of a Fisher distribution is located at a pole of the sphere (e.g., $\alpha = 0$, β arbitrary) then the distributions in θ and ϕ are independent and separable. In that case, the marginal distribution in ϕ is the circular uniform distribution, while the marginal distribution in θ is given by

$$f(\theta) = \kappa \sin\theta \frac{e^{\kappa\cos\theta}}{e^{\kappa} - e^{-\kappa}}. \quad (10)$$

The maximum likelihood estimate of the mean direction is given by the sample mean direction [14]. Experimental data may require estimators for the concentration parameter κ that are robust against outliers, or have been modified for small $(N < 16)$ sample sizes [15]-[18]. However, because neither are issues here, we simply used the maximum likelihood estimator,

$$\coth\kappa - \frac{1}{\kappa} = \frac{R}{N}, \quad (11)$$

that is given in [10]. The Fisher distributions with concentration parameters κ that best fit the simulated data sets corresponding to selected values of K between $-\infty$ and 20 dB and ρ_{pwr} between 0 and 0.9 are shown in Figure 3. We first decimated the data to ensure that the samples were independent and then performed a pair of tests to assess: (1) the uniformity of the marginal distribution in longitude ϕ and (2) the goodness-of-fit of the marginal distribution in co-latitude θ to the exponential component of the Fisher distribution [15]. Because the parameters of the proposed distributions have been estimated from simulated data, we have used standard test statistics that have been modified as described in [19] and [20].

Our first task was to verify that the simulated data is rotationally symmetric. Let X_i be a random sample from a hypothesized distribution $F(x)$, and let $X_{(i)}$ be the order statistics of the sample so that $X_{(1)} \leq ... \leq X_{(N)}$. Following [14], we compared the value of Kuiper's test statistic,

$$\begin{aligned} V_N = &\max\left[\frac{i}{N} - F\left(X_{(i)}\right)\right] \\ &+ \max\left[F\left(X_{(i)}\right) - \frac{i-1}{N}\right] \end{aligned} \quad (12)$$

for $i = 1, ..., N$, modified for the case when the distribution is continuous and completely specified (in this case uniform) by

$$V = V_N\left(\sqrt{N} + 0.155 + \frac{0.24}{\sqrt{N}}\right) \quad (13)$$

to standard values presented in [20], and were able to accept the hypothesis of rotational symmetry at the 15% significance level for all values of K and ρ considered.

We then assessed the fit of the probability distribution in (10) to the marginal distribution of the data in θ. Following [14] once again, we compared the value of the Kolmogorov-Smirnov test statistic,

$$\begin{aligned} D_N = \max\Bigg[&\max\left[\frac{i}{N} - F\left(X_{(i)}\right)\right], \\ &\max\left[F\left(X_{(i)}\right) - \frac{i-1}{N}\right]\Bigg] \end{aligned} \quad (14)$$

modified for the case when the distribution is exponential with estimated parameters as

$$D = \left(D_N - \frac{0.2}{N}\right)\left(\sqrt{N} + 0.26 + \frac{0.5}{\sqrt{N}}\right) \quad (15)$$

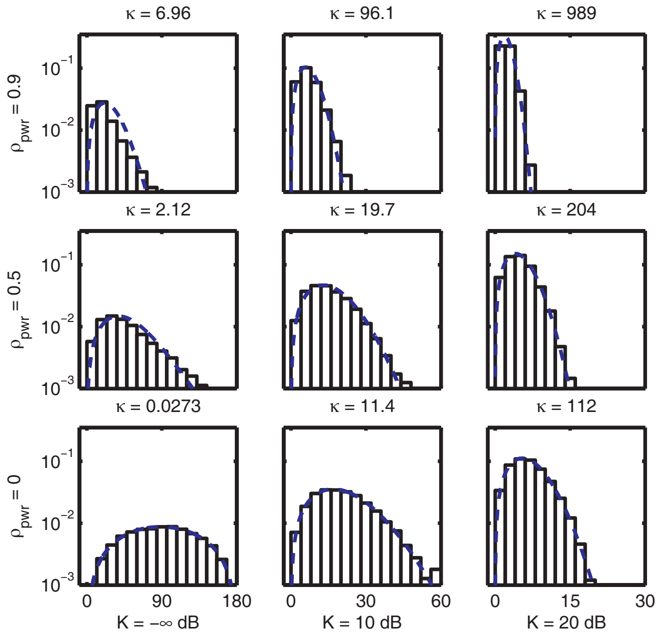

Fig. 3. The Fisher distributions that best fit the co-latitude component of the polarization state distribution for selected values of K between $-\infty$ and 20 dB and ρ_{pwr} between 0 and 0.9.

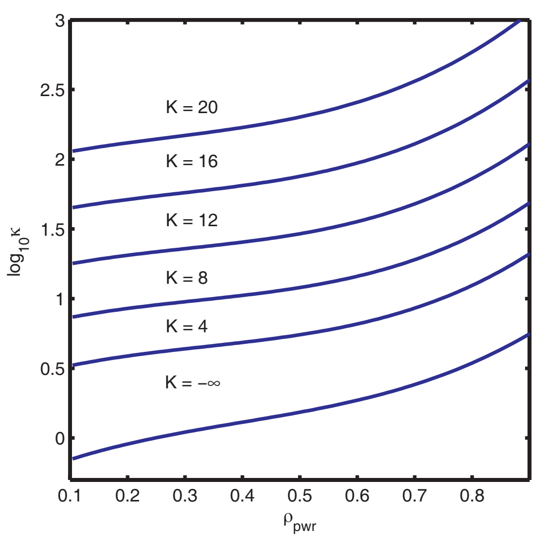

Fig. 4. The Fisher concentration parameter κ as a function of the cross-correlation coefficient, ρ_{pwr}, between the orthogonally polarized diversity branches and the Ricean K-factor K [dB] that characterizes fading on each diversity branch.

to standard values presented in [20], and confirmed what is apparent from visual inspection of Figure 3: The Fisher distribution fits the simulated data well for most values of K and ρ_{pwr} but slightly over predicts the polarization state dispersion in the unlikely case that the fading distribution is close to Rayleigh while the branches are also highly correlated.

In Figure 4, we show the manner in which the logarithmic form of the concentration parameter depends upon K and ρ_{pwr}. As K increases, the variation in the polarimetric ratio decreases so $\log_{10}\kappa$ also increases, i.e., the polarization state distribution becomes more concentrated. A similar effect occurs as ρ_{pwr} increases and the instantaneous amplitudes of the signals on the two branches become more similar. To facilitate estimation of the concentration parameter given the narrowband channel parameters, we generated a polynomial response surface that models the relationship between $\log_{10}\kappa$ and the parameters K and ρ_{pwr}. A third order polynomial surface provides a good fit with an RMS error of 0.04 while a fourth order surface only reduces the error to 0.02 at the expense of far greater complexity. The third order model is given by

$$\begin{aligned}\log_{10}\kappa =& \beta_0 + \beta_1 K + \beta_2\rho_{pwr} + \beta_3 K\rho_{pwr} \\ &+ \beta_4 K^2 + \beta_5\rho_{pwr}^2 + \beta_6 K\rho_{pwr}^2 \\ &+ \beta_7 K^2\rho_{pwr} + \beta_8 K^3 + \beta_9\rho_{pwr}^3,\end{aligned} \tag{16}$$

where

$$\beta = \begin{vmatrix} 0.1133868 \\ 0.0677943 \\ 1.3392816 \\ -0.0303603 \\ 0.0021740 \\ -2.4102017 \\ 0.0276632 \\ 0.0007400 \\ -0.0000464 \\ 2.2787705 \end{vmatrix} \tag{17}$$

and K is expressed in dB.

IV. Prediction of XPD from Narrowband Channel Parameters

Although previous experimental work has shown that XPD is correlated with Ricean K-factor [21], eqn. (9) indicates that the spread of polarization states that determines XPD is actually determined by κ. The results of the last section indicate that κ is determined by both K and ρ_{pwr}. In order to determine how effectively we can predict XPD given κ, K or ρ_{pwr}, we synthesized a multiplicity of fading diversity signals with values of K between $-\infty$ and 20 dB and ρ_{pwr} between 0 and 0.9 and estimated both the corresponding κ and XPD. We found that XPD is more highly correlated with $\log_{10}\kappa$ (correlation = 0.97) than with K or ρ_{pwr} alone (correlation = 0.58 and 0.60 respectively). The relationship between κ and XPD is shown in Figure 5 and is given by

$$\text{XPD [dB]} = 9.82\log_{10}\kappa + 15.05. \tag{18}$$

Together, (16) and (18) allow XPD to be accurately predicted directly from narrowband channel model parameters of the sort described in [1].

V. Conclusion

We have shown by simulation that when the fading signals observed on polarization diversity branches are Ricean distributed, the first-order distribution of polarization states is generally well-approximated by a Fisher distribution with specified concentration parameter, κ. Although one generally needs to measure the phase between diversity branches to determine the received polarization state at a given instant, the concentration parameter κ is a function of the narrowband channel parameters K and ρ_{pwr}, both of which can be

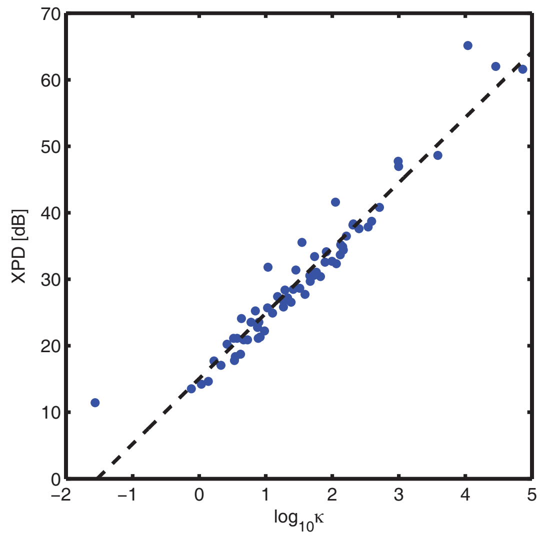

Fig. 5. Cross-polar discrimination as a function of the Fisher concentration parameter κ. The correlation coefficient between κ and XPD is 0.97.

estimated from simple measurements of received power vs. time. We have also shown that κ is a better indicator than K or ρ_{pwr} alone of the level of cross-polar discrimination (XPD) on the channel, a parameter useful to those engaged in the development and evaluation of polarization re-use or polarized MIMO schemes. In order to simplify interpretation of the results, we have assumed what we refer to as an ideal Ricean fading diversity channel in which the average path gains and Ricean K-factors on both orthogonally polarized diversity branches are identical. We will relax this restriction in the next phase of our study where we will consider how unequal path gains and/or K-factors affect the polarization state distribution.

REFERENCES

[1] D. G. Michelson, V. Erceg, and L. J. Greenstein, "Modeling diversity reception over narrowband fixed wireless channels," *IEEE MTT-S Int. Topical Symp. Technol. Wireless Applic.*, 1999, pp. 95-100.

[2] D. J. Cichon, T. Kurner, and W. Wiesbeck, "Polarimetric aspects in antenna related superposition of multipath signals," in *Proc. ICAP*, 1993, pp. 80-83.

[3] M. M. McKinnon, "Three-dimensional statistics of radio polarimetry," *Astrophys. J. Suppl.*, vol. 148, no. 2, pp. 519-526, Oct. 2003.

[4] V. R. Anreddy and M. A. Ingram, "Capacity of measured Ricean and Rayleigh indoor MIMO channels at 2.4 GHz with polarization and spatial diversity," in *Proc. IEEE WCNC*, 2006, pp. 946-951.

[5] H. Bolcskei, R. U. Nabar, V. Erceg, D. Gesbert, and A. J. Paulraj, "Performance of spatial multiplexing in the presence of polarization diversity," in *Proc. IEEE ICASSP*, 2001, pp. 2437-2440.

[6] J. R. Mendes, M. D. Yacoub, and D. Benevides da Costa, "Closed-form generalised power correlation coefficient of Ricean channels," *Eur. Trans. Telecommun.*, vol. 18, pp. 403-409, 2007.

[7] Y. Karasawa and H. Iwai, "Modeling of signal envelope correlation of line-of-sight fading with applications to frequency correlation analysis," *IEEE Trans. Commun.*, vol. 42, no. 6, pp. 2201-2203, 1994.

[8] W. L. Stutzman, *Polarization in Electromagnetic Systems.* Boston: Artech House, 1993.

[9] B. Natarajan, C. R. Nassar, and V. Chandrasekhar, "Generation of correlated Rayleigh fading envelopes for spread spectrum applications," *IEEE Commun. Lett.*, vol. 4, no. 1, pp. 9-11, Jan. 2000.

[10] R. Fisher, "Dispersion on a sphere," *Proc. R. Soc. London, Ser. A*, vol. 217, no. 1130, pp. 295-303, May 1953.

[11] G. Ulrich, "Computer generation of distributions on the m-sphere," *Appl. Statist.*, vol. 33, no. 2, pp. 158-163, 1984.

[12] A. T. A. Wood, "Simulation of the von Mises Fisher distribution," *Commun. Statist. - Simula.*, vol. 23, no. 1, pp. 157-164, 1994.

[13] N. I. Fisher, T. Lewis, and M. E. Willcox, "Tests of discordancy for samples from Fisher's distribution on the sphere," *Appl. Statist.*, vol. 30, no. 3, pp. 230-237, 1981.

[14] N. I. Fisher, T. Lewis, and B. J. J. Embleton, *Statistical Analysis of Spherical Data.* Cambridge Univ. Press, 1987.

[15] K. V. Mardia and P. E. Jupp, *Directional Statistics.* New York: Wiley, 2000.

[16] P. L. McFadden, "The best estimate of Fisher's precision parameter κ," *Geophys. J. R. Astr. Soc.*, vol. 60, pp. 97-407, 1980.

[17] D. J. Best and N. I. Fisher, "The bias of the maximum likelihood estimators of the von Mises-Fisher concentration parameters," *Commun. Statist.*, vol. B10, pp. 493-502, 1981.

[18] N. I. Fisher, "Robust estimation of the concentration parameter of Fisher's distribution on the sphere," *Appl. Statist.*, vol. 31, no. 2, pp. 152-154, 1982.

[19] N. I. Fisher and D. J. Best, "Goodness-of-fit tests for Fisher's distribution on the sphere," *Austral. J. Statist.*, vol. 26, no. 2, pp. 151-159, 1984.

[20] M. A. Stephens, "EDF statistics for goodness of fit and some comparisons," *J. Amer. Statistical Assoc.*, vol. 69, no. 2, pp. 730-737, Sept. 1974.

[21] D. S. Baum, D. Gore, R. Nabar, S. Panchanathan, K. V. S. Hari, V. Erceg, and A. J. Paulraj, "Measurement and characterization of broadband MIMO fixed wireless channels at 2.5 GHz," in *Proc. IEEE ICPWC*, 2000, pp. 203-206.